Postprint version (author-accepted manuscript) of Corrado De Pascali *et al.*, "3D-printed biomimetic artificial muscles using soft actuators that contract and elongate". *Sci. Robot.***7**, eabn4155(2022).
DOI:10.1126/scirobotics.abn4155

Muscle-like geometry-based actuators for a new generation of bioinspired machines

Authors:

Corrado De Pascali[1,2]*, Giovanna Adele Naselli[1]†, Stefano Palagi[1,2]†, Rob B. N. Scharff[1], Barbara Mazzolai[1]*

Affiliations:

[1]Bioinspired Soft Robotics Laboratory, Istituto Italiano di Tecnologia; Genoa, Italy.

[2]The BioRobotics Institute, Scuola Superiore Sant'Anna; Pontedera, Italy.

*Corresponding author. Email: Corrado.depascali@iit.it; Barbara.mazzolai@iit.it

†These authors contributed equally to this work.

Abstract:

Biomimetic machines able to integrate with natural and social environments will find ubiquitous applications, from biodiversity conservation to elderly daily care. Although machines' man-made actuators have reached exceptional performances, the versatility of natural muscles and the grace of the movements realized by their complex arrangements remain largely unmatched. Here we present a new class of artificial muscles, the GRACEs, that can contract and extend by design, as described by a mathematical model, and can be realized at different dimensional scales and with different materials and mechanical performances, enabling a wide range of lifelike movements. The GRACEs can be fabricated through low-cost additive manufacturing and even built directly

within functional devices, thus democratizing artificial muscle technologies and biomimetic machines. The GRACEs will therefore enable the distributed development and widespread deployment of biomimetic machines that integrate in our world.

One-Sentence Summary:

A novel class of versatile and 3D-printable artificial muscles aims at making machines more lifelike and accessible.

Main Text:

Introduction

All muscles in the animal kingdom consist of bundles of uniaxially contractile fibers, in turn made of identical sarcomere units, yet muscles are not at all equal. They have sizes spanning three orders of magnitude (from meters down to millimeters), a variety of shapes and architectures (i.e., spatial distributions of fibers within the muscle), and complex arrangements within the body (including antagonistic pairs), enabling the dexterity and wide ranges of movement amplitudes, speeds, and forces observed in animals (*1*, *2*). Muscles represent therefore a reference for actuators in artificial machines, not only because of their remarkable performances in terms of force, power and durability (which have been met and even surpassed (*3*, *4*)) but, especially, for their astonishing versatility, which is still largely unmatched (*5*–*8*) (Fig. 1A).

Actuators that are designed to perform muscle-like contraction are known as *artificial muscles* (*9*, *10*). Pneumatic artificial muscles (PAMs), which contract upon pressurization, were firstly introduced in the 1950s and usually consist of a flexible or stretchable cylindrical membrane that is constrained by high tensile-resistant fibers and capped by two rigid end fittings (*11*–*14*). The

fibers and fittings are needed as they translate the membrane's volume increase (and consequent radial expansion) into a longitudinal contraction (*15*–*19*). Starting from the traditional PAMs, pneumatics has widely spread in soft robotics, particularly to reproduce the muscle's behavior in bioinspired robots (*20*, *21*). Within the soft robotics field, numerous novel pneumatic actuators were developed, becoming lighter and less expensive (*22*), achieving multiple possible deformations (*23*), improving their compactness (*24*), or drastically reducing their radial size (*25*, *26*). In spite of these recent results, the layout of PAMs still involves a number of assembled components, inherently hindering miniaturization, implementation of non-fusiform-like architectures (required for complex lifelike movements), and, last but not least, the wide adoption and customization of artificial muscle technologies (*27*). Therefore, radically novel and simpler PAM designs are needed that are amenable to dimensional scaling, customization to specific needs, and fabrication by accessible additive manufacturing techniques (*28*–*30*) (Fig. 1B). These will contribute to democratizing artificial muscles applications and will allow artificial machines to move with grace and dexterity akin to those of animals and humans.

Here we propose a novel class of PAMs made of just one monolithic element: a membrane with an engineered shape. The membrane geometry inherently implements the coupling of inflation to axial contraction, with no need of tensile-resistant components, end caps or constraints (Fig. 1C). Moving from the concept of pleats-guided deformation, partially exploited also in a traditional class of PAMs named Pleated PAMs (*31*, *32*), we iteratively designed and prototyped pleated-membrane structures such as to achieve muscle-like axial contraction upon pressurization-driven unfolding of the pleats – with no need for strain-limiting elements or end caps. The obtained general parametric geometry represents the starting point for designing actuators that contract

and/or elongate, inherently enabling antagonistic operation. For this reason, we named our artificial muscles GRACE: GeometRy-based Actuators that Contract and Elongate.

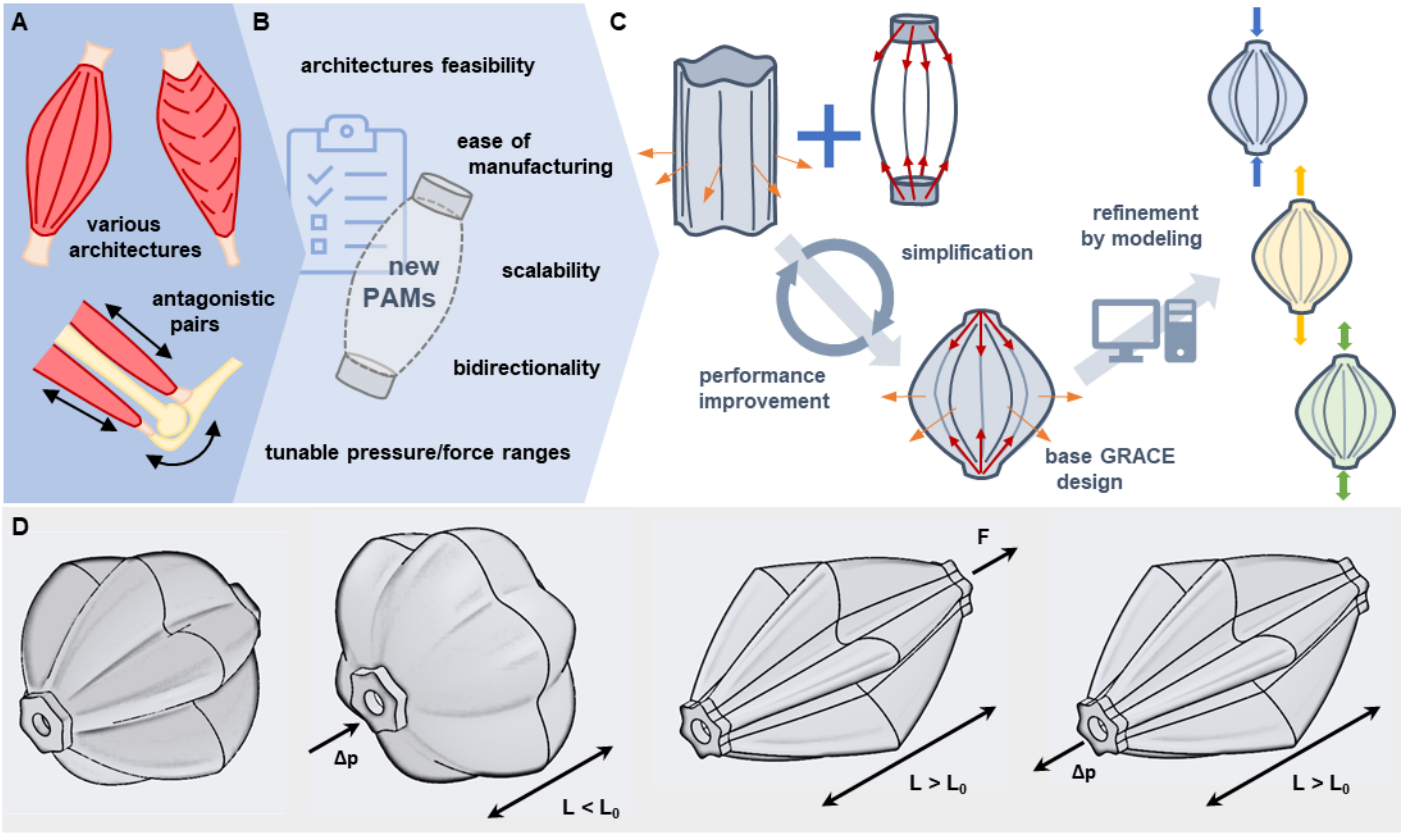

Fig. 1. GRACE muscles concept. (A) Skeletal muscles vary widely in size, architecture, and performance, and are inherently suited to antagonistic operation. (B) Analogously, we aimed at developing new PAMs that are easy to manufacture (thus allowing for scalability and feasibility of complex architectures), bidirectional (thus well suited for antagonistic operation), and have input pressure and output force ranges that are tunable. (C) We developed a base design that intrinsically couple radial expansion and axial contraction in a single monolithic pleated membrane (without the need for strain-constraining elements). By further refining this design, we developed a number of different actuators with different behaviors and performance. (D) Operating principle of the GRACEs: contraction, passive and active elongation.

Results

Here we show that the GRACEs are highly effective (stroke above 30%, load/weight ratios from hundreds up to over thousands – depending on the membrane material, Fig. 2A-B and movie S1), yet convenient and extremely versatile artificial muscles: they can maximize contraction, elongation or antagonistic actuation by design, they can be fabricated in different materials (Fig. S4), with different low-cost 3D printers and at various scales (Fig. 2C and movie S2), and they can be seamlessly built-in in complex devices enabling sophisticated and diverse movements.

All these features are enabled by the GRACEs operating principle: a low-strain geometrical transformation of the actuators' structure. The GRACEs consist of a continuum thin shell having a curvilinear shape, narrowing at the two extremities, and longitudinal engineered pleats. When pressurized, the actuator expands radially as the pleats unfold circumferentially (with no substantial stretch of the membrane), and the two extremities are brought together to the middle resulting in a longitudinal contraction (Fig. 1D, second one from left). Contrarily, upon depressurization the pleats fold, leading to radial contraction and consequent longitudinal elongation (Fig. 1D, first one from right). Unlike in the so-called Pleated PAMs (*31*, *32*), here the pleats are shaped to inherently enable the contraction and/or elongation of the monolithic GRACEs, with no need for constraining components. In the GRACEs the curvilinear profiles of the pleats and the overall actuator's shape are key, whereas in the PPAMs the pleats only played a secondary role in the actuation. They eased the circumferential expansion of the actuator's inner membrane, reducing the membrane stretch present in the conventional McKibben's design, though without altering the contraction principle that similarly relied on tensile resistant fibers.

Fig. 2. GRACE muscles (A)A 4-cm-long, 6-g GRACE-C made of Flexible 80A (SLA) lifts up a 1-kg load for 20% of its length. (B) A 4-cm-long, 8-g GRACE-C made of Flexfill 98A (FDM) lifts up a 8-kg load for 20% of its length. (C) GRACE-Cs of sizes spanning one order of magnitude.

As shown in Fig. S1A, the central cross section of a GRACE consists of a closed series of elliptical arcs whose concavity alternates to generate the pleats. The GRACE results from lofting such cross section along longitudinal parabolic curves (Fig. S1B), up to the end section on both sides. We compute the deformed configuration of the GRACE by setting an optimization problem, in which the enclosed volume (Fig. S1C) is maximized for contraction and minimized for extension. Our approach is purely geometrical (see Supplementary Information), as the lengths of all the parabolic and elliptical arcs are required to remain unchanged under actuation. In other words,

we treated the GRACE as an inextensible membrane with null thickness. Normalization of all lengths ensures that the results are valid at any scale.

We used our model to investigate how the shape of the pleats influences the GRACE's behavior. The model allows to consider any number of pleats. Here, for brevity, we discuss the results obtained for 40,320 different GRACEs design with 6 pleats, having computed their maximum contraction (Fig. 3A) and elongation (Fig 3B). The profiles that perform better in contraction are those with narrow ellipses and deep pleats, which can largely expand when the GRACE is inflated (we will denote this design by GRACE-C). On the contrary, if actuators that perform deflation-driven elongation are desired, the required GRACEs designs are characterized by shallow pleats (GRACE-E). If, instead, actuators are needed that perform best in antagonistic configuration, a suitable geometry is found that performs well both in elongation and contraction (GRACE-A). Fig. 3C shows the central cross section of the three obtained GRACE versions, highlighting that the GRACE-A profile lies between the GRACE-C and the GRACE-E. The same process can be followed to find optimal geometries for a different number of pleats (see Supplementary Text for additional results). Generally speaking, the same considerations hold; narrow and deep pleats promote the contraction, while the opposite is found for the extension. However, the role played by each geometrical parameter, and by their relative proportion, is difficult to grasp by pure intuition.

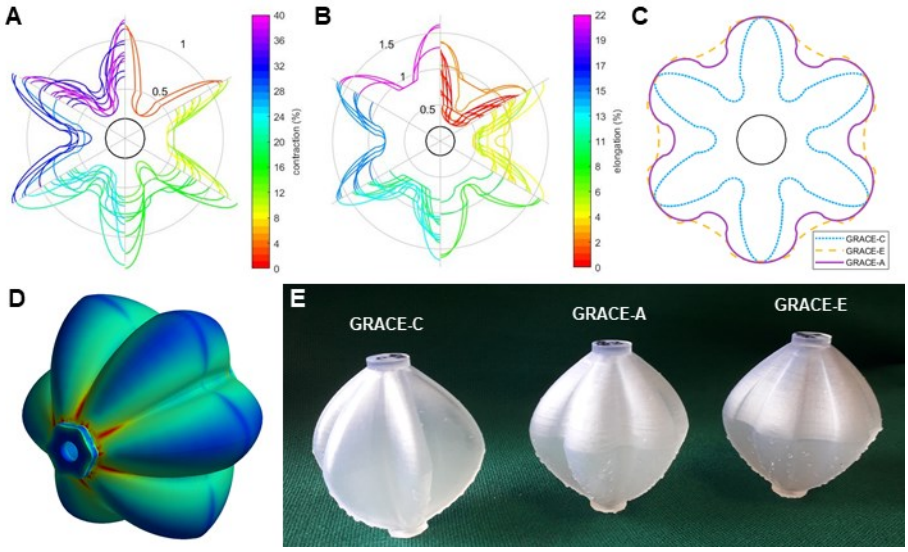

Fig. 3. GRACE multiparametric model (A) Contraction and (B) elongation (as percentage of initial length) for different profiles. (C) Central cross section of GRACE-C (maximizing Contraction), GRACE-E (maximizing Elongation) and GRACE-A (maximizing bidirectional actuation, best suited for Antagonistic operation). (D) Maximum principal stress distributions for GRACE-C muscle during isometric contraction resulting from the FEA. (E) 3D printed samples of the three GRACE designs.

Based on the parameters obtained for the three versions of the GRACEs (Supplementary Table 1) and setting the desired length (40 mm for most actuators), we defined their actual designs, identifying suitable wall thickness and material through Finite Element Analysis (FEA – Fig. 3D and S4). We thus simulated the force exerted by the actuators, as well as the membrane stress and strain distributions, at given input pressures for different thicknesses and material elastic moduli. Starting from a homogeneous thickness of 1 mm (convenient for our intended manufacturing technology), we found that materials with an elastic modulus of about 5 MPa would ensure the desired contraction/elongation and considerable forces (in the order of tens of N) at conveniently low pressures (order of tenths of bar). We thus simulated actuators made

with an available material having properties in this range (Formlabs Flexible 80A) and locally refined the walls thickness to reduce stress concentrations (Fig. 3D). Simulating free contraction and elongation conditions (contraction and elongation without constraints or loads applied), we found contractions and elongations slightly smaller and larger, respectively, than those predicted by the model and maximum local strains below 30% (Fig. S5) for all considered versions of the GRACEs. Notably, the simulations indicate that the operating pressure ranges and resulting output forces of the GRACEs can be increased by simply using stiffer materials and/or making the membrane thicker (see Supplementary Information).

We directly printed the different GRACEs by low-cost desktop 3D printers and commercial materials (Fig. 3E). We first characterized the GRACEs by tensile tests (stretching, Fig. S6D). The GRACE-A exhibits the lowest initial tensile stiffness (about half of that of the GRACE-C and comparable to that of the GRACE-E), which allows it to be easily stretched by the contraction of an antagonistic muscle. This confirms what we observed in simulations (see Supplementary Text and Fig. S6): the GRACE-As are better suited for antagonistic operation (especially at low pressures/deformations) than the other designs. This advantage is further enhanced by the possibility of assisting the contraction of a muscle by extending its antagonist *actively* (through depressurization).

We then investigated the contraction (+20 kPa) and extension (−10 kPa) of the different GRACEs by isotonic (constant force) and isometric (constant length) tests. In the isotonic tests (movie S3), we applied and held three different tensile loads (0 N – free actuation, 4 N, and 8 N) while subjecting the actuators to five cycles of pressure and measuring their shortening/elongation (see Supplementary Text). The GRACE-C samples performed about 25% free contraction and showed decreasing shortening at increasing loads (Fig. 4A-B and S7). For

the GRACE-A samples, instead, the shortening increased with increasing loads, up to 17.5% with 8 N (Fig. S9), as the load stretches the actuators, slightly folding the pleats and thus increasing the unfolding range. The GRACE-A samples also showed about 20% free extension (just slightly lower than that of the GRACE-Es) and elongation decreasing with increasing load (Fig. S11). Overall, the GRACE-As exhibit an actuation range (shortening + elongation) of 25% to 30% (Fig. 4C), slightly higher than the shortening of the GRACE-Cs. In the isometric tests (movie S4), we applied and held three different values of fixed stretch (0 mm – blocking force, 4 mm, and 8 mm,) while applying five cycles of pressure and measuring the output forces. The GRACE-C samples exerted a blocking force of 17 N and a maximum pulling force of ~18 N with a 4-mm stretch (Fig. 4D-E and S8). In contraction, the GRACE-A samples performed a blocking force of ~7 N and pulling forces increasing with the applied stretch up to ~14 N (Fig. S10). In extension, they achieved a 7.5 N blocking force and a pushing force peaking to 9.5 N with the 4-mm stretch (Fig. S12).

Compared to skeletal muscles, the GRACEs we tested here exhibit similar deformations and lower forces. The shortening of the GRACE-Cs is comparable to the typical values for muscles (~20%), while the actuation range of the GRACE-As approaches the maximum range achievable by muscles (>40%) (*3*, *4*). Both GRACE-C and GRACE-A samples showed contraction forces lower than the ones typically exerted by muscles of equivalent diameter (~10^2 N) (Fig. 4F) (*3*, *4*), yet these can be achieved by GRACEs fabricated with stiffer materials, thicker membrane and actuated with higher pressures (see Fig. S4 and movie S1). Therefore, force performance is limited by the specific material we used in the characterization, not by the GRACEs design.

The adopted material, however, is advantageous in studying the GRACEs as it is inherently photoelastic (its refraction index changes in response to local stresses). Through a plane

polariscope setup we captured the stress-induced fringe patterns during both isometric and isotonic actuation (Fig. 4G-H and movie S5). The outcomes allowed us both to visualize that SLA process did not generate any substantial residual stress in the fabricated structures and to collect feedback on the results from FEA, improving the design refinement phase. Indeed, the observed color patterns qualitatively match the stress distributions from the FEA, showing a certain stress concentration in the inward pleats near the two extremities, which led us to preemptively refine the membrane thickness locally to avoid premature failure of the actuators.

We then challenged our 3D-printed actuators with 1000 cycles of free contraction or extension (Fig. 4I and S16). The GRACE-C consistently reached 26% shortening (compared to initial length) and the GRACE-A consistently achieved 12% shortening and ~20% elongation. No failure or permanent changes were observed during the tests, suggesting that, even if fabricated with a low-cost desktop 3D printer and a commercial material, the GRACEs can easily withstand many actuation cycles. We also tested the GRACE-C for 20 actuation cycles with input frequencies spanning from 0.066 Hz to 1 Hz to examine its dynamical behavior (results reported in Fig. S15), which, nonetheless, strongly depend on the whole pneumatic driving system.

Postprint version (author-accepted manuscript) of Corrado De Pascali *et al.*, "3D-printed biomimetic artificial muscles using soft actuators that contract and elongate". *Sci. Robot.***7**, eabn4155(2022).
DOI:10.1126/scirobotics.abn4155

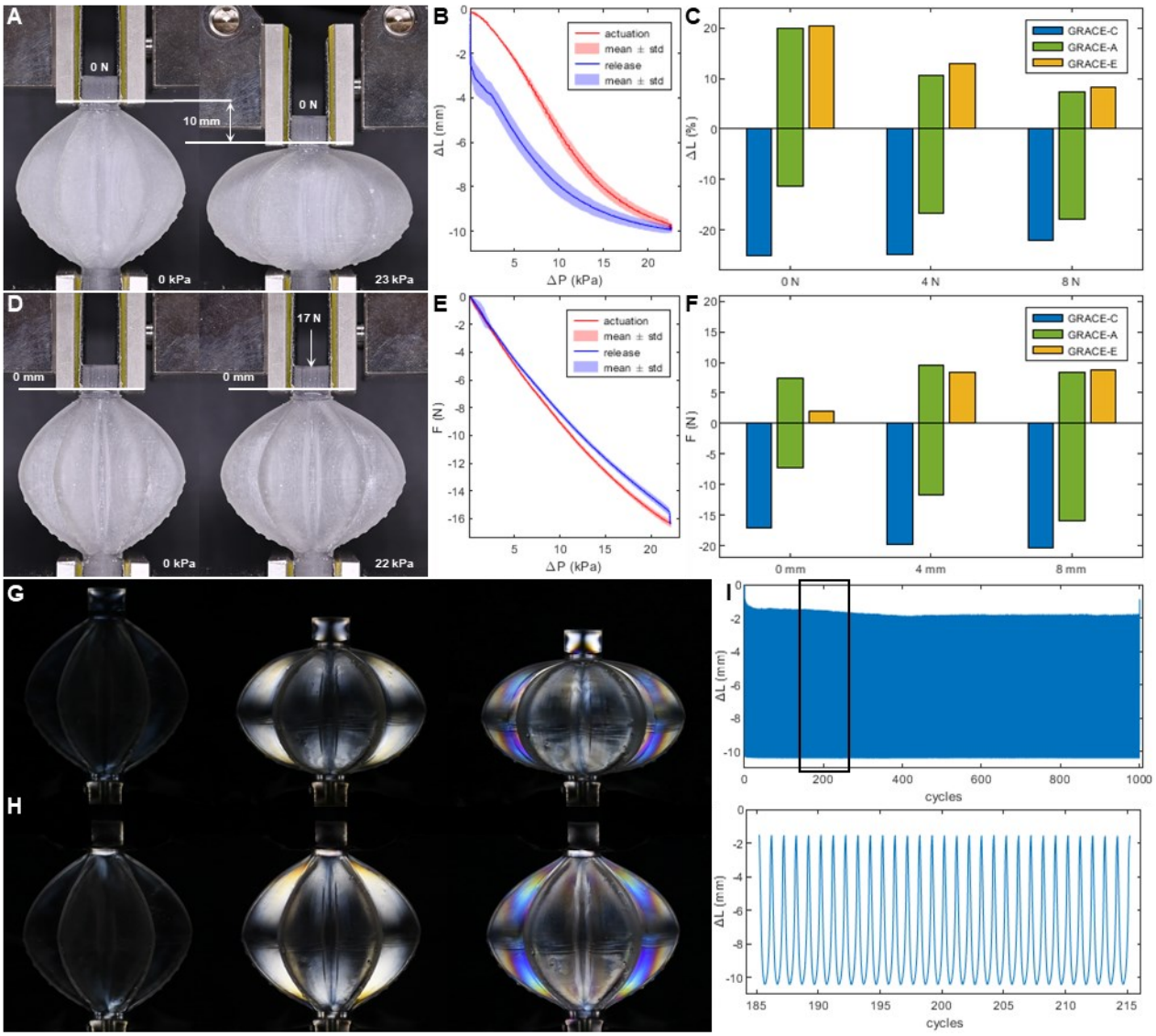

Fig. 4. GRACE muscles characterization and durability. GRACE-C no-load isotonic tests: (A) rest state (left) and inflated state (right); (B) actuation (inflation) and release (deflation) curves (mean over five cycles and five samples). (C) Shortening/elongation of the three designs in isotonic tests at different loads. GRACE-C no-stretch isometric tests: (D) rest (left) and inflated (right) states; (E) actuation and release curves (mean over five cycles and five samples). (F) Pulling/pushing force of the three designs in isometric tests at different stretches. Stress distribution in GRACE-Cs revealed by photoelasticity during (G) a no-load isotonic test and (H) a no-stretch isometric test. (I) No-load cycling of a GRACE-C: the initial length is not recovered within the relaxation phase of the cycles (15 s, overpressure linearly ramping down to zero), most likely because of the material's viscoelasticity, yet it is recovered at the end of the test.

Although they exhibit remarkable performance, the characterizing feature of the GRACEs is their extreme versatility. To showcase some of it, we 3D-printed a full GRACE-based 'pneumatic hand' that consists of a palm, 5 fingers with built-in tendons and flexible joints, and a mobile wrist. We developed this demonstrator to show the wide variety of smooth movements that can be enabled by exploiting GRACEs in series, in parallel, in antagonistic configurations, of different sizes, and directly embedded in a complex functional structure. The full hand has overall dimensions of 180 mm×160 mm×50 mm. Remarkably, it was directly 3D-printed as a single-material monolithic structure, without any need of assembling and ready to be plugged with pressure lines (Fig. 5E and S19), demonstrating that the GRACEs enable the one-step fabrication of actuated devices. The hand contains 18 GRACEs of different sizes and kinds: 14 20-mm-long GRACE-Cs in the hand palm and 4 30-mm-long GRACE-As in the wrist. Each finger can move independently through a tendon pulled by three (two for the thumb) GRACE-Cs in series (Fig. 5A). The wrist has a central fixed pillar and four GRACE-As on the sides and showcases the antagonistic operation of the GRACEs. For instance, contracting two adjacent muscles and extending the other two make the hand rotate around the directions parallel to the base plane (Fig. 5B-C, S21-22-and movie S6). Each finger joint reaches around 25° bending angle while the wrist achieves ±15° and ± 30° around the axis perpendicular and parallel to the hand palm, respectively. The richness of movements of the monolithic GRACE-hand (Fig. 5D-E and movie S7) just gives a hint of the sophistication of lifelike movements that could be achieved thanks to the unparalleled versatility of the GRACEs. It also demonstrates that the GRACEs can make the development of functional devices and prototypes accessible to anyone with a desktop 3D printer.

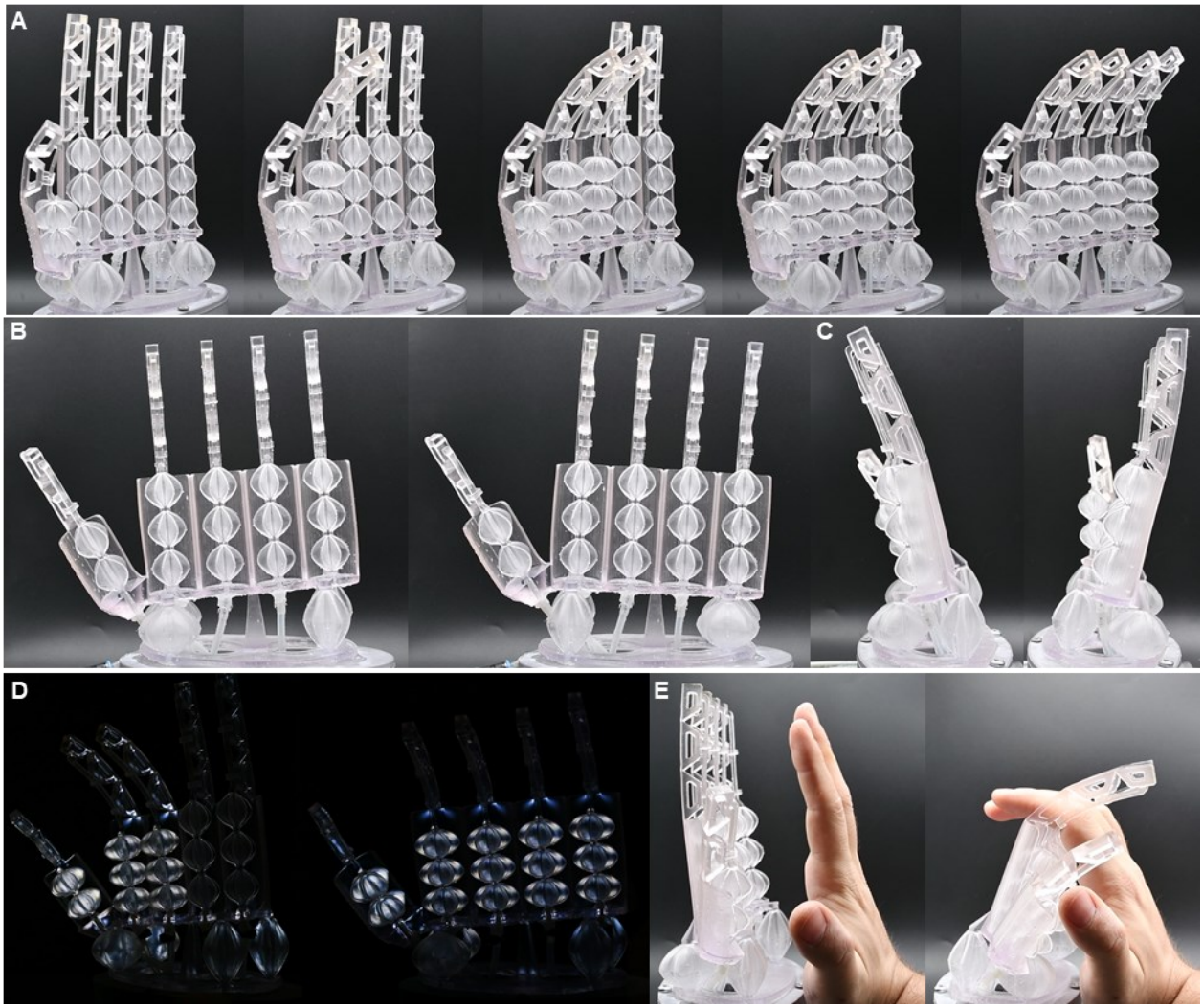

Fig. 5. The GRACE hand. (A) Fingers at rest and actuated while the wrist is at rest. (B, C) Rotational movements enabled by the bidirectional bending of the wrist. (D) Actuation of the embodied GRACEs highlighted by photoelasticity. (E) Lifelike movement of the GRACE hand.

Conclusions

Our results demonstrate that the GRACEs are an extremely versatile and easily fabricated new class of pneumatic artificial muscles The GRACEs have overall performances akin to those of state-of-the-art pneumatic artificial muscles (Table S3), yet they show a substantially higher

level of versatility. Their actuation behavior can be tuned at will, their size can be scaled significantly, and their actuation strength can be changed substantially. Based on each specific application of the GRACEs, it is possible to define the best specific design considering the required performance and size constraints. For instance, the puffy shape of the GRACEs, which is shared by all designs generated with the model, makes them apparently bulkier than other PAMs of the same length and may represent a problem in some applications where compactness is crucial. This, however, can be easily overcome by scaling down and arranging several GRACEs in series, without increasing the manufacturing effort (as we did in the hand palm for actuating the fingers). Indeed, the monolithic design of the GRACEs enables for the first time the direct 3D-printing of artificial muscles and functional pneumatic devices in one step. The GRACEs therefore enable the realization of complex actuated structures with sophisticated lifelike movements that could facilitate the integration of biomimetic machines in our world. Moreover, the GRACEs development process, consisting of modelling, FEA-based refinement, and additive manufacturing steps, is amenable to automated mass customization, allowing for the straightforward and parallel production of different GRACEs on demand (Fig. S18). During both the characterization and the 1000-cycles test, we experienced no specific weaknesses related to their 3D-printed structure; however, a contraction force limit could show up for the ones manufactured through FDM due to the adhesion strength between the layers, which could only be overcome by their parallel arrangement. Future more in-depth studies on their behavior depending on different materials and additive manufacturing processes involved should be carried out. Nevertheless, we expect that thanks to their versatile design, they will conveniently conform to new insights on additive manufacturing techniques and materials. In future works, we will realize bioinspired machines exploiting the GRACEs to mimic the diversified muscles arrangements present in the animal kingdom. At the same time, the GRACEs will make

biomimetic devices accessible to anyone with a low-cost desktop 3D printer, thus contributing to the democratization and wide adoption of lifelike machines.

Materials and Methods

GRACE design and Finite Elements Models

The GRACE designs were carried out using Solidworks CAD software and the finite element method simulations were performed by importing the corresponding STL files into ANSYS software. Through static structural analysis accounting for large displacements, we simulated the behaviors of the three representative GRACE designs, refined their wall thicknesses in order to reduce local stress concentrations, and predicted the forces exerted for different material properties. All materials were modeled with a linear elastic behavior whose properties (secant Young's Modulus and Poisson ratio) were extrapolated from the corresponding datasheets. We set the Poisson ratio equal to 0.4 for all the TPU/TPE materials and resins we simulated. For the Flexible 80A material, we set 5 MPa Young's Modulus, 6 MPa for the FlexMark 7, 10 MPa for the FlexMark 8, 12 MPa for the NinjaFlex, 30 MPa for the Filaflex, 33 MPa for the Flexfill 92A, 35 MPa for the FlexMark 9 and 46 MPa for the Flexfill 98A. The meshes involved tetrahedral elements of 0.5 mm main dimension and are built using the cyclic symmetrical property of the designs starting from one pleat. We employed two different set of boundary conditions for the simulations: one end of the GRACE muscle fixed while the other free with an applied constant load to reproduce the isotonic conditions; one end of the GRACE muscle fixed while the other stretched with a constant displacement to reproduce the isometric conditions. The pressure inputs were applied as a linear function of time with ten steps.

Fabrication

To realize GRACE samples, we adopted several commercial materials through two additive manufacturing techniques, fused deposition method (FDM) and stereolithography (SLA). For FDM we employed the Prusa I3 MK3S, and for the SLA we used both the Form 2 and the Form 3 from Formlabs. For the manufacturing with Prusa printer, we used NinjaFlex® (Shore Hardness 85A) filaments, produced by NinjaTek, Flexmark®7-8-9 (Shore Hardness 70A, 81A, 93A) by Treed, FlexFill® (Shore Hardness 92A, 98A) from Prusa Research, and FilaFlex40® (Shore Hardness 40D) by FilaTech, while two different versions of the same photopolymer resin, Flexible v2® (85A) and the new Flexible 80A® both by Formlabs, for the Form 2.

To fabricate the samples for the characterization and the pneumatic hand (Fig. S18), we chose stereolithography-based 3D printing (SLA, Formlabs Form 2 and Form 3) because of both high resolution and wide range of printable structure sizes but other desktop 3D printers can be used as well.

Characterization

To characterize the GRACEs, we carried out three isotonic (0 N, 4 N, 8 N) and three isometric tests (0 mm, 4 mm, 8 mm) for each of the three main designs, doubled in the case of the antagonistic design for contraction and extension, for a total of 24 tests. For each test, we employed 5 samples. The samples were held in a Zwick/Roell Z005 testing machine with a 50N loadcell to record the displacement and the force (Fig. S17). Through the testing machine we applied and maintained constant stretching forces during isotonic tests and stretching displacements during isometric tests. The samples were pressurized by a compressor and depressurized by a vacuum pump, connected, respectively to a pressure regulator and a vacuum

regulator, both controlled by a wave generator. The overpressure was measured with a pressure sensor and the de-pressure by a vacuum sensor, both connected to a National Instrument board. For each test, we applied five cycles of trapezoidal wave voltage input from the wave generator to the regulators in order to generate a trapezoidal wave of pressure with five cycles. We set different length time parameters for the wave of the isotonic tests and the isometric ones. Their lengths were chosen after having determined the characteristic time constants of the viscoelastic behavior of the material, by previous creep and stress relaxation tests on dog bones samples. In this way, there was enough time between the cycles to allow the sample to return to its starting condition (relaxation time > 5 corresponding characteristic times, 3 min for isotonic tests and 5 min for isometric tests) and to ensure that the actuation time was short enough to avoid high viscoelastic behaviors (each cycle ramp < 1 corresponding characteristic time, 30s for isotonic tests and 1 min for isometric tests).

Photoelasticity

The experimental setup is shown (Fig. S23). The linear polarized light emitted from the LCD screen passes through the GRACE sample or the pneumatic hand. A linear polarizer film that is crossed with respect to the transmission orientation of the LCD is adopted as analyzer and a camera is used to capture the resulting color map.

1000-cycles test and dynamical test

In the 1000-cycles tests, we employed the same setup as for the characterization tests but with different inputs to the regulators. The inputs were triangular waves without relaxing time between each cycle with a period of 30s (15s each ramp). As for the isotonic test with no load applied, the testing machine was involved only to record the displacement while keeping the

force applied null. In the dynamical test, we replaced the testing machine with the Aurora tracking system (magnetic tracking), that was better able to follow higher frequency deformations. We applied triangular wave inputs as for the 1000-cycles test but with frequency spanning from 0.066 Hz to 1 Hz.

3D-printed artificial hand setup

To actuate the artificial hand with automated sequences of motion, we built a dedicated pneumatic circuit (Fig. S20) and control the electro-valves through an Arduino Mega board. For the GRACE-C embedded in the five fingers, we employed five 2/2 electro-valves, one for each finger, and one overpressure regulator. For the four GRACE-A of the wrist, we employed four 3/2 electro-valves in order to switch from pressurization to depressurization, four 2/2 electro-valves to open and close the inlet inputs, one overpressure regulator and one vacuum regulator. Each finger was actuated with pressure inputs of 20 kPa while 16 kPa input was adopted for the contracting GRACE-As and –8 kPa input for the actively elongating ones

Supplementary Materials

Supplementary Text

Figs. S1 to S23

Tables S1 to S3

Movies S1 to S7

References and Notes

1. A. A. Biewener, Biomechanics of mammalian terrestrial locomotion. *Science (80-.).* **250**, 1097–1103 (1990).

2. M. H. Dickinson, C. T. Farley, R. J. Full, M. A. R. Koehl, R. Kram, S. Lehman, How animals move: an integrative view. *Science (80-.).* **288**, 100–106 (2000).

3. I. W. Hunter, S. Lafontaine, A comparison of muscle with artificial actuators. *Tech. Dig. IEEE Solid-State Sens. Actuator Work.*, 178–185 (1992).

4. J. D. Madden, N. Vandesteeg, P. A. Anquetil, P. G. Madden, A. Takshi, Z. Rachel, S. R. Lafontaine, P. A. Wieringa, I. W. Hunter, Artificial muscle technology: physical principles and naval prospects. *IEEE J. Ocean. Eng.* **29**, 706–728 (2004).

5. J. Kim, J. W. Kim, H. C. Kim, L. Zhai, H. U. Ko, R. M. Muthoka, Review of soft actuator materials. *Int. J. Precis. Eng. Manuf.* **20**, 2221–2241 (2019).

6. A. Miriyev, A focus on soft actuation. *Actuators*. **8**, 74 (2019).

7. E. Acome, S. K. Mitchell, T. G. Morrissey, M. B. Emmett, C. Benjamin, M. King, M. Radakovitz, C. Keplinger, Hydraulically amplified self-healing electrostatic actuators with muscle-like performance. *Science (80-.).* **359**, 61–65 (2018).

8. H. Wang, P. York, Y. Chen, S. Russo, T. Ranzani, C. Walsh, R. J. Wood, Biologically inspired electrostatic artificial muscles for insect-sized robots. *Int. J. Rob. Res.* **40**, 895–922 (2021).

9. D. Yang, M. S. Verma, J. H. So, B. Mosadegh, C. Keplinger, B. Lee, F. Khashai, E. Lossner, Z. Suo, G. M. Whitesides, Buckling pneumatic linear actuators inspired by muscle. *Adv. Mater. Technol.* **1**, 31–33 (2016).

10. G. K. Klute, J. M. Czerniecki, B. Hannaford, McKibben artificial muscles: pneumatic actuators with biomechanical intelligence. *IEEE/ASME Int. Conf. Adv. Intell. Mechatronics, AIM*, 221–226 (1999).

11. F. Daerden, D. Lefeber, B. Verrelst, R. Van Ham, Pleated pneumatic artificial muscles: actuators for automation and robotics. *IEEE/ASME Int. Conf. Adv. Intell. Mechatronics, AIM*. **2**, 738–743 (2001).

12. S. Krishna, T. Nagarajan, A. M. A. Rani, Review of current development of pneumatic artificial muscle. *J. Appl. Sci.* **11**, 1749–1755 (2011).

13. G. Andrikopoulos, G. Nikolakopoulos, S. Manesis, A survey on applications of pneumatic artificial muscles. *2011 19th Mediterr. Conf. Control Autom. MED 2011*, 1439–1446 (2011).

14. S. Terryn, J. Brancart, D. Lefeber, G. Van Assche, B. Vanderborght, Self-healing soft pneumatic robots. *Sci. Robot.* **2**, 1–13 (2017).

15. F. Daerden, D. Lefeber, Pneumatic artificial muscles: actuators for robotics and automation. *Eur. J. Mech. Environ. Eng.* **47**, 11–21 (2002).

16. J. Bishop-Moser, S. Kota, Design and modeling of generalized fiber-reinforced pneumatic soft actuators. *IEEE Trans. Robot.* **31**, 536–545 (2015).

17. A. Miriyev, K. Stack, H. Lipson, Soft material for soft actuators. *Nat. Commun.* **8**, 1–8 (2017).

18. D. Rus, M. T. Tolley, Design, fabrication and control of soft robots. *Nature*. **521**, 467–475 (2015).

19. D. Trivedi, C. D. Rahn, W. M. Kier, I. D. Walker, Soft robotics: biological inspiration, state of the art, and future research. *Appl. Bionics Biomech.* **5**, 99–117 (2008).

20. C. Laschi, B. Mazzolai, M. Cianchetti, Soft robotics: Technologies and systems pushing the boundaries of robot abilities. *Sci. Robot.* **1**, 1–11 (2016).

21. S. Coyle, C. Majidi, P. LeDuc, K. J. Hsia, Bio-inspired soft robotics: Material selection, actuation, and design. *Extrem. Mech. Lett.* **22**, 51–59 (2018).

22. R. S. Diteesawat, T. Helps, M. Taghavi, J. Rossiter, Characteristic Analysis and Design Optimization of Bubble Artificial Muscles. *Soft Robot.* **8**, 186–199 (2021).

23. P. H. Nguyen, W. Zhang, Design and Computational Modeling of Fabric Soft Pneumatic Actuators for Wearable Assistive Devices. *Sci. Rep.* **10**, 1–13 (2020).

24. Y. L. Park, J. Santos, K. G. Galloway, E. C. Goldfield, R. J. Wood, A soft wearable robotic device for active knee motions using flat pneumatic artificial muscles. *Proc. - IEEE Int. Conf. Robot. Autom.*, 4805–4810 (2014).

25. S. Kurumaya, H. Nabae, G. Endo, K. Suzumori, Design of thin McKibben muscle and multifilament structure. *Sensors Actuators, A Phys.* **261**, 66–74 (2017).

26. S. Kurumaya, K. Suzumori, H. Nabae, S. Wakimoto, Musculoskeletal lower-limb robot driven by multifilament muscles. *ROBOMECH J.* **3**, 1–15 (2016).

27. D. R. Higueras-Ruiz, M. W. Shafer, H. P. Feigenbaum, Cavatappi artificial muscles from drawing, twisting, and coiling polymer tubes. *Sci. Robot.* **6** (2021).

28. T. J. Wallin, J. Pikul, R. F. Shepherd, 3D printing of soft robotic systems. *Nat. Rev. Mater.* **3**, 84–100 (2018).

29. B. N. Peele, T. J. Wallin, H. Zhao, R. F. Shepherd, 3D printing antagonistic systems of artificial muscle using projection stereolithography. *Bioinspiration and Biomimetics*. **10** (2015).

30. M. Schaffner, J. A. Faber, L. Pianegonda, P. A. Rühs, F. Coulter, A. R. Studart, 3D printing of robotic soft actuators with programmable bioinspired architectures. *Nat. Commun.* **9**, 878 (2018).

31. F. Daerden, thesis, Vrije Universiteit Brussel (1999).

32. D. Villegas, M. Van Damme, B. Vanderborght, P. Beyl, D. Lefeber, Third-generation pleated pneumatic artificial muscles for robotic applications: development and comparison with Mckibben muscle. *Adv. Robot.* **26**, 1205–1227 (2012).

Acknowledgments: We thank our colleagues Dr. Alessio Mondini (Istituto Italiano di Tecnologia), Dr. Francesco Visentin (Istituto Italiano di Tecnologia) and Dr. Carlo Filippeschi (Istituto Italiano di Tecnologia) for the technical assistance and supervision provided during the fabrication and the experimental characterization processes. **Funding:** This work has received funding from the European Union's Horizon 2020 research and innovation program under grant agreement No. 863212 (PROBOSCIS project). **Author contributions:** C.D.P., S.P., and G.A.N. conceived the GRACE concept. G.A.N developed the geometrical model. C.D.P designed and fabricated the GRACE samples and the 3D

printed pneumatic hand. C.D.P conducted the mechanical characterization. C.D.P and R.B.N.S carried out the photoelastic experiments and built the pneumatic hand control setup. C.D.P and S.P. analyzed the experimental data. B.M. supervised the work and provided insights on the muscle physiology. All authors contributed to the writing of the paper.

Competing interests: C.D.P, G.A.N, S.P. and B.M. have a patent pending application on the GRACE design. **Data and materials availability:** All data needed to support the conclusions of this manuscript are included in the main text or the Supplementary Materials. The GRACE geometric model (MATLAB script) and data set resulting from the GRACE characterization will be publicly available on Zenodo upon acceptance.